Emission and propagation of sound waves in porous media with active inner heat sources

Rodolfo Venegas, Claude Boutin, Gabriel Núñez

Emission and propagation of sound waves in porous media with active inner heat sources

Rodolfo Venegas[1]
University Austral of Chile
Institute of Acoustics, P.O. Box 567, Valdivia, Chile

Claude Boutin[2]
Université de Lyon - Ecole Nationale des Travaux Publics de l'Etat,
LGCB / LTDS UMR-CNRS 5513 / CeLyA, Rue Maurice Audin, Vaulx-en-Velin 69518, France

Gabriel Núñez[3]
University Austral of Chile
Institute of Acoustics, P.O. Box 567, Valdivia, Chile

ABSTRACT

Wave propagation through porous media with active inner heat sources is investigated in this paper. Through the use of the two-scale asymptotic method of homogenisation, it is found that a macroscopic non-homogeneous wave equation describes the emission and propagation of sound waves in such active porous media. The upscaled model is verified numerically for the cases of single and double porosity media, and shows that the general properties of the effective parameters of the porous media are not altered by the inner heat sources. Instead, the inner heat sources contribute to the non-homogeneous term in the upscaled wave equation. This paper also explores the potential of using active inner heat sources in porous media for controlling incident sound waves in a practical scenario.

1. INTRODUCTION

Acoustics of rigid-frame porous media with active inner heat sources is studied in this paper. These heterogeneous media, in their simplest form, comprise a solid frame and a single fluid-saturated pore network in which externally-actuated volumetric heat sources are placed. More complex materials, such as double porosity composites with heat sources in the pore fluid network of the most permeable constituent, are also investigated. The two-scale asymptotic method of homogenisation [1] is used to establish the macroscopic description of emission and propagation of sound waves in rigid-frame periodic porous media with active inner volumetric heat sources.

[1]rodolfo.venegas@uach.cl

[2]claude.boutin@entpe.fr

[3]gabriel.nunez@alumnos.uach.cl

The phenomenon of sound directly produced by heat is the subject of study of thermoacoustics [2]. A great deal of research has reported theoretical and/or experimental results on the acoustic emission, due to heat sources, by thermophones made of either solid or porous materials [3–7]. Several attempts to correctly model this acoustic emission phenomenon in porous media have been reviewed in [8]. However, none of the reviewed models reduces to the classical upscaled model of wave propagation in rigid-frame porous media [1, 9–11] when the heat sources are off. Another instance in which heat sources are of use is in photoacoustic spectrometry [12]. This is a technique in which a modulated light beam impinging a sample can heat it up and cool it down in a cycle and, depending on how fast the cycle is, sound can be produced. Well established applications of photoacoustic spectrometry are trace gas analysis and spectroscopy of solid surfaces [12]. This non-exhaustive account of literature, together with recent investigations on sound propagation in metamaterials in which the changes in or gradients of temperature affect their acoustical properties, e.g. [13, 14], provide further motivation for the present study.

This work generalises the theories of acoustic wave propagation in rigid-frame single porosity [1, 9–11] and double porosity composite materials [15, 16] by accounting for active inner heat sources in such materials. For the sake of simplicity, only local volumetric heat sources as forcing terms are considered in this work. However, other internal mechanisms of thermal excitation are possible and their study is a matter of future work.

The format of the paper is as follows. The upscaled theory of wave emission and propagation in porous media with volumetric heat sources is presented in § 2. This includes the analysis of the effective parameters and sources arising in the upscaling process. In § 3, the acoustic properties of a novel effective parameter and those of the different effective sources are discussed, along with the numerical verification of the theory and some examples of acoustic descriptors of rigidly-backed layers of active porous media. Concluding remarks are presented in the last section of the paper.

2. THEORY

2.1. Geometry and general assumptions

Figure 1 shows a schematic diagram of the geometry of a single porosity air-saturated porous medium with identical volumetric heat sources Q placed in the pore fluid network Ω_f. The porosity of the material is $\phi = \Omega_f/\Omega$, where Ω is the total volume of the material, Γ is the fluid-solid interface, and $\mathbf{n}$ is the outward-pointing vector normal to Γ. The period of the material is ℓ and the macroscopic characteristic size L is related to the sound wavelength λ through $\lambda = 2\pi L$. Long-wavelength regime is considered, which means that $\lambda \gg \ell$. This ensures a large separation of scale, quantified through a small parameter $\varepsilon = \ell/L \ll 1$, and the existence of a representative elementary volume Ω. Harmonic dependence of the type $e^{j\omega t}$, where ω is the angular frequency and t represents the time, is adopted.

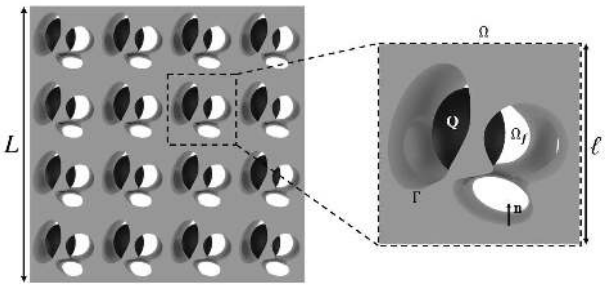

Figure 1: Scheme of the geometry of a porous medium with active inner heat sources in the pore fluid network.

2.2. Local description

The local equations that govern the propagation of sound waves in a single porosity rigid-frame material are the linearised equations of conservation of momentum (Equation 1), mass (Equation 2), and energy (Equation 3), and the equation of state (Equation 4), i.e.

$$\mathrm{div}(2\eta\mathbf{D}(\mathbf{v})) - \nabla p = \mathrm{j}\omega\rho_0\mathbf{v} \quad \text{in} \quad \Omega_f, \tag{1}$$

$$\mathrm{j}\omega\frac{\rho}{\rho_0} + \nabla\cdot\mathbf{v} = 0 \quad \text{in} \quad \Omega_f, \tag{2}$$

$$\nabla\cdot\kappa\nabla\tau - \mathrm{j}\omega\rho_0 c_p\tau = -\mathrm{j}\omega p - Q \quad \text{in} \quad \Omega_f, \tag{3}$$

$$\frac{p}{P_0} = \frac{\rho}{\rho_0} + \frac{\tau}{\tau_0} \quad \text{in} \quad \Omega_f. \tag{4}$$

In these equations, p, τ, and ρ represent, respectively, the excess of pressure, temperature, and density, while $\mathbf{v}$ is the fluid velocity and $\mathbf{D}(\mathbf{v}) = (\nabla\mathbf{v} + (\nabla\mathbf{v})^T)/2$ is the strain rate tensor. The Fourier-transformed volumetric heat source in Ω_f is Q. This can represent, for example, a modulated laser beam injecting energy in the system and working at an angular frequency ω. The subscript 0 denotes mean values of the physical quantities in the fluid. For example, τ_0 is the mean value of the fluid temperature over an acoustic cycle. The saturating air has a dynamic viscosity η, thermal conductivity κ, and specific heat capacity at constant pressure c_p. Due to the varying temperature of the saturating fluid, these are taken as the mean value of the respective quantities.

To close the system, the conditions of adherence and impenetrability as well as zero excess temperature are formulated on the impervious solid boundary Γ, i.e.

$$\mathbf{v} = 0 \quad \text{on} \quad \Gamma, \tag{5}$$

$$\tau = 0 \quad \text{on} \quad \Gamma. \tag{6}$$

2.3. Outline of the homogenisation procedure

The homogenisation procedure is outlined in this section. The details of the derivation will be reported elsewhere.

The long-wavelength regime imposes that the pressure and the divergence of the velocity vary macroscopically [1, 9, 10], while the fluid velocity and its rate of deviatoric strain fluctuate locally. The latter is also the case for the excess temperature. Furthermore, it is assumed that the volumetric heat source term Q varies locally. Considering these assumptions, a dimensional analysis then leads to $|\nabla p| = O(\check{p}/L)$, $|\nabla\cdot\mathbf{v}| = O(\check{v}/L)$, $|\mathrm{div}(2\eta\mathbf{D}(\mathbf{v}))| = O(\eta\check{v}/\ell^2)$, and $|\kappa\nabla\cdot\nabla\tau| = O(\kappa\check{\tau}/\ell^2)$, where the accent $\check{}$ indicates a characteristic value of the variable it is applied to. For example, $\check{\tau}$ is a characteristic value of the excess temperature. Regarding the relative order of magnitude of the terms in Equations 1 to 4, the case of interest is where all the terms in each equation are of the same order of magnitude. In turn, this leads to the following estimates $O(\eta\check{v}/\ell^2) = O(\omega\rho_0\check{v}) = O(\check{p}/L)$, $O(\check{v}/L) = O(\omega\check{\rho}/\rho_0)$, $O(\check{p}/P_0) = O(\check{\tau}/\tau_0) = O(\check{\rho}/\rho_0)$, and $O(\kappa\check{\tau}/\ell^2) = O(\omega\rho_0 c_p\check{\tau}) = O(\omega\check{p}) = O(\check{Q})$. The latter estimates reflect that the thermal conduction and inertial terms balance the source due to pressure and the volumetric heat source.

Introducing two independent spatial variables, i.e. x and $y = \varepsilon^{-1}x$, which respectively account for macroscopic and local fluctuations, noting that the differential operator becomes $\nabla = \nabla_x + \varepsilon^{-1}\nabla_y$, and following the usual rescaling procedure, the differential operators in the first terms on the left-hand sides of Equations 1 and 3 are rescaled by ε^2 to reflect that both the velocity and excess temperature vary locally. Then, inserting into the rescaled equations the unknown variables written as expansion

series in terms of the small parameter ε and further matching the terms with the same ε powers, one obtains a series of local boundary-value problems. The resolution of these problems enables the calculation of the effective parameters and sources of the active material.

With regard to fluid flow, it is found that the leading-order pressure $p^{(0)}$ is a macroscopic variable since $\nabla_y p^{(0)} = \mathbf{0}$, and the leading-order velocity $\mathbf{v}^{(0)}$ and $p^{(1)}$ are governed by the same classical oscillatory Stokes problem, formulated in the pore fluid network, as that for porous media without heat sources.

The equations that govern the leading-order excess temperature $\tau^{(0)}$ are Equations 3 and 6 with $\nabla \to \nabla_y$, $\tau \to \tau^{(0)}$ and $p \to p^{(0)}$. The solution of this linear boundary-value problem forced by two terms, i.e. the locally constant leading-order pressure and the locally fluctuating volumetric heat source, is given by a linear combination of the solutions of the problem when the sources separately excite the fluid saturating the material, that is

$$\tau^{(0)} = \tau_p + \tau_q, \quad \text{with} \quad \tau_p = \frac{\tilde{\theta}_p(y,\omega)}{\kappa}(\mathrm{j}\omega p^{(0)}) \quad \text{and} \quad \tau_q = \frac{\tilde{\theta}_q(y,\omega)}{\kappa}(\langle Q\rangle_f), \tag{7}$$

where τ_p and τ_q are the excess temperatures generated by the pressure and volumetric heat sources, respectively; the averaging operator is defined as $\langle\cdot\rangle_f = \frac{1}{\Omega_f}\int_{\Omega_f}\cdot\, d\Omega$, and the local fields $\tilde{\theta}_\iota$ (with $\iota = p, q$) are the solution of the following boundary-value problems

$$\nabla_y^2\tilde{\theta}_\iota - \mathrm{j}\delta_t^{-2}\tilde{\theta}_\iota = \begin{cases} -1 & \text{for} \quad \iota = p \\ -\frac{Q}{\langle Q\rangle_f} & \text{for} \quad \iota = q. \end{cases} \quad \text{in} \quad \Omega_f, \tag{8}$$

$$\tilde{\theta}_\iota = 0 \quad \text{on} \quad \Gamma, \tag{9}$$

where $\delta_t = \sqrt{\kappa/\omega\rho_0 c_p}$ is the thermal boundary layer thickness.

Then, i) spatially averaging the leading-order equation of conservation of mass, ii) applying the divergence theorem together with the conditions of periodicity and zero velocity on Γ, and iii) making use of the equation of state and the expression of the leading-order excess temperature, one obtains a macroscopic non-homogeneous mass balance equation. This equation and the classical dynamic Darcy's law govern the emission and propagation of sound waves in an air-saturated porous medium with volumetric heat sources actuating in the pore fluid network. This macroscopic description is now detailed.

2.4. Macroscopic description

The macroscopic description is given by the macroscopic non-homogeneous mass balance equation and the dynamic Darcy's law, i.e. (with $\phi\langle\cdot\rangle_f = \langle\cdot\rangle$)

$$\nabla_x \cdot \langle\mathbf{v}^{(0)}\rangle + \mathrm{j}\omega p^{(0)}\mathsf{C} = H(\omega), \tag{10}$$

$$\langle\mathbf{v}^{(0)}\rangle = -\frac{\mathbf{k}(\omega)}{\eta}\cdot\nabla_x p^{(0)} \quad \text{or} \quad \mathrm{j}\omega\boldsymbol{\rho}(\omega)\cdot\langle\mathbf{v}^{(0)}\rangle = -\nabla_x p^{(0)}, \tag{11}$$

where $\mathbf{k}(\omega)$ is the dynamic viscous permeability, $\boldsymbol{\rho}(\omega)$ is the effective density, and $\mathsf{C}(\omega)$ is the effective compressibility which is given by (with $\theta_p = \langle\tilde{\theta_p}\rangle$)

$$\mathsf{C}(\omega) = \mathsf{C}_p(\omega) = \frac{\phi}{P_0}\left(1 - \frac{\gamma-1}{\gamma}\left(\frac{\theta_p(\omega)}{-\mathrm{j}\phi\delta_t^2}\right)\right), \tag{12}$$

where $\theta_p = \langle\tilde{\theta_p}\rangle$ is the classical dynamic thermal permeability [10].

The macroscopic effective volumetric source $H(\omega)$ is defined as

$$H(\omega) = \langle Q\rangle_f \frac{\phi}{P_0}\frac{\gamma-1}{\gamma}\left(\frac{\theta_q(\omega)}{-\mathrm{j}\phi\delta_t^2}\right). \tag{13}$$

Here, $\theta_q = \langle \tilde{\theta}_q \rangle$ acts as a filter of the volumetric heat source and represents the thermal response of the saturating fluid to a locally varying, instead of constant, source.
Remarks:
- The general properties of the effective parameters, i.e. the dynamic viscous permeability and effective compressibility, are not altered by the volumetric heat sources. The latter only contribute to the effective volumetric source term $H(\omega)$.
- The microstructure of the material acts as a filter, represented by the novel effective parameter θ_q, of the volumetric heat source. Moreover, the homogenisation process reveals that the volumetric heat source Q is transformed into a macroscopic effective volumetric source $H(\omega)$ acting as a forcing term in the macroscopic mass balance equation.
- The emission of sound by the active porous medium is driven by the effective source term $H(\omega)$. The physical origin of such emission is not related to the usual generation of sound by fluid flux but rather to acoustic density variations induced by the extra local temperature field, i.e. τ_q, generated by the volumetric heat sources.
- Consistently, the macroscopic description of wave propagation in a porous medium without heat sources is retrieved when $H(\omega) = 0$.
- The effective parameter θ_p is the classical dynamic thermal permeability [10]. Its behaviour in frequency is as follows. At frequencies much lower than the thermal characteristic frequency $\omega_t = \phi\kappa/\rho_0 c_p \theta_{p0}$, where θ_{p0} is the static thermal permeability, θ_p tends to θ_{p0} while for $\omega \gg \omega_t$, one has that $\theta_p = -\mathrm{j}\phi\delta_t^2$. These correspond to leading-order asymptotic values.
- The limiting leading-order values of θ_q have the same mathematical form than those of θ_p. However, it is stressed that, in general, $\theta_q \neq \theta_p$. Consequently, $\theta_{q0} \neq \theta_{p0}$ and the ratio ω_q/ω_t, where ω_q is a specific thermal characteristic frequency, can be estimated as $O(\theta_{p0}/\theta_{q0})$.
- The macroscopic description of emission and propagation of sound waves in a double porosity composite with both highly contrasted matrix and inclusion permeabilities and inner heat sources placed in the pore fluid network of the most permeable matrix has the same mathematical form as that of Equations 10 and 11. However, i) the dynamic viscous permeability is given by $\mathbf{k} = \varphi_m \mathbf{k}_m \cdot \boldsymbol{\alpha}_\infty^{-1}$, where φ_m is the volume fraction of the matrix of permeability $\mathbf{k}_m$ and $\boldsymbol{\alpha}_\infty$ is the tortuosity tensor induced by the presence of the highly resistive inclusions [15, 16]; ii) the effective source term is $\varphi_m H(\omega)$; and iii) the effective compressibility C becomes $\varphi_m \mathsf{C}_m + (1-\varphi_m)\mathsf{C}_i\mathcal{F}$, where C_i (respectively C_m) is the effective compressibility of the much less (respectively more) permeable inclusion (respectively matrix), and $\mathcal{F}$, defined as the ratio between the averaged pressures in the less and much permeable pore fluid networks, accounts for pressure diffusion [15–18].

2.5. Non-homogeneous wave equation

For simplicity, macro-isotropy is considered, meaning that $\mathbf{k} = \mathcal{K}\mathbf{I}$ and $\boldsymbol{\rho} = \rho\mathbf{I}$, where $\mathbf{I}$ is the identity tensor. Inserting Equation 11 into Equation 10 results in the following non-homogeneous Helmholtz equation

$$\nabla_x^2 p^{(0)} + k_c^2(\omega) p^{(0)} = \mathcal{S}(\omega), \tag{14}$$

where the effective wave number is given by $k_c = \omega\sqrt{\rho(\omega)\mathsf{C}(\omega)}$ and the source term $\mathcal{S}(\omega)$ reads as (with $c_0 = \sqrt{\gamma P_0/\rho_0}$ being the adiabatic speed of sound in air)

$$\mathcal{S}(\omega) = -\mathrm{j}\omega\rho(\omega)H(\omega) = -\mathrm{j}\omega\langle Q\rangle \frac{\rho(\omega)}{\rho_0}\frac{\gamma-1}{c_0^2}\left(\frac{\theta_q(\omega)}{-\mathrm{j}\phi\delta_t^2}\right). \tag{15}$$

Using the asymptotic values for the parameters θ_q, θ_p and $\rho(\omega \ll \omega_v) = \eta/\mathrm{j}\omega\mathcal{K}_0$ and $\rho(\omega \gg \omega_v) = \rho_0\alpha_\infty/\phi$, where $\omega_v = \phi\eta/\rho_0\mathcal{K}_0\alpha_\infty$ is the Biot frequency, $\mathcal{K}_0$ is the static viscous permeability, and α_∞ is the tortuosity, the following limiting values for the wave number and source term can be derived

(with $\mathrm{N_{Pr}} = \eta c_p/\kappa$ being the Prandtl number and $\mathcal{D}_0 = P_0\mathcal{K}_0/\phi\eta$ the pressure diffusivity)

$$k_c(\omega \ll \omega_v) = \sqrt{\frac{-\mathrm{j}\omega}{\mathcal{D}_0}} \quad \text{and} \quad \mathcal{S}(\omega \ll \omega_v) = -\mathrm{j}\omega\frac{\gamma-1}{c_0^2}\mathrm{N_{Pr}}\frac{\theta_{q0}}{\mathcal{K}_0}\langle Q\rangle_f, \tag{16}$$

$$k_c(\omega \gg \omega_v) = \frac{\omega}{c_0/\sqrt{\alpha_\infty}} \quad \text{and} \quad \mathcal{S}(\omega \gg \omega_t) = -\mathrm{j}\omega\frac{\gamma-1}{c_0^2/\alpha_\infty}\langle Q\rangle_f. \tag{17}$$

Equation 16 shows that, at low frequencies, Equation 14 becomes a non-homogeneous diffusion equation with diffusivity $\mathcal{D}_0$ and effective source term $\mathcal{S}(\omega \ll \omega_v)$. On the other hand, Equation 17 reveals that at high frequencies, where the effects of viscosity and heat conduction can be disregarded, Equation 14 is a non-homogeneous wave equation with effective speed of sound $c_0/\sqrt{\alpha_\infty}$ and source term $\mathcal{S}(\omega \gg \omega_t)$. This resulting equation becomes the classical non-homogeneous wave equation in free space with a heat source since, in such a case, $\alpha_\infty = 1$ (see equation 7.1.23 in [19] with $\langle Q\rangle_f = \rho\epsilon$ in their notation).

Since $\mathcal{S}$ is constant with respect to the macroscopic spatial variable, a particular solution of Equation 14 determining the acoustic pressure $\mathfrak{p}(\omega)$ emitted by the active porous medium is found as

$$\mathfrak{p}(\omega) = \frac{\mathcal{S}(\omega)}{k_c^2} = \frac{H(\omega)}{\mathrm{j}\omega\mathsf{C}(\omega)} = \frac{1}{\mathrm{j}\omega\mathsf{C}(\omega)}\frac{\langle Q\rangle}{P_0}\frac{\gamma-1}{\gamma}\frac{\theta_q(\omega)}{-\mathrm{j}\phi\delta_t^2} = \frac{\langle Q\rangle_f}{\mathrm{j}\omega}\frac{\frac{\gamma-1}{\gamma}\frac{\theta_q(\omega)}{-\mathrm{j}\phi\delta_t^2}}{1-\frac{\gamma-1}{\gamma}\frac{\theta_p(\omega)}{-\mathrm{j}\phi\delta_t^2}}. \tag{18}$$

Hence, the following limiting values are obtained

$$\mathfrak{p}(\omega \ll \omega_q) = \frac{\langle Q\rangle_f}{\mathrm{j}\omega}\frac{\frac{\gamma-1}{\gamma}\frac{\theta_{q0}}{-\mathrm{j}\phi\delta_t^2}}{1-\frac{\gamma-1}{\gamma}\frac{\theta_{p0}}{-\mathrm{j}\phi\delta_t^2}} \approx \langle Q\rangle_f\frac{\theta_{q0}}{\phi}\frac{\gamma-1}{\gamma}\frac{\rho_0 c_p}{\kappa}, \quad \text{and} \quad \mathfrak{p}(\omega \gg \omega_t) = \frac{\langle Q\rangle_f}{\mathrm{j}\omega}(\gamma-1). \tag{19}$$

These equations predict a constant magnitude of the pressure emitted by the porous medium at low frequencies and a $1/\omega$ decrease at high frequencies.

3. RESULTS

Figure 2 shows the geometry of a regularly-arranged array of cylinders, which serves as a model for a fibrous material with fibre radius a and porosity $\phi = 1 - \pi a^2/b^2$, where b is the cell size. A volumetric heat source, representing a modulated Gaussian beam, is placed in the pore fluid network of the unit cell. In cylindrical coordinates, this is given by $Q = Q_a e^{\mathrm{j}\varphi} e^{-r^2/s^2}$, where s is a parameter that controls the width of the beam, Q_a is the amplitude of the heat source, and φ is the relative phase between the local temperature fields τ_p and τ_q. A value of $\varphi = 0$ means that τ_p and τ_q are in phase, while $\varphi = \pi$ indicates that τ_p and τ_q are out of phase.

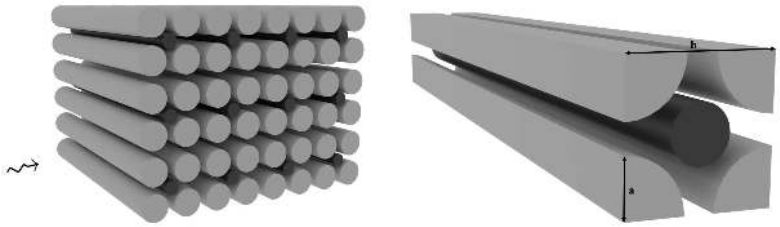

Figure 2: Scheme of the geometry (left) and unit cell (right) of an air-saturated array of regularly-arranged solid circular cylinders (in grey) with volumetric heat sources (in black) in the pore space. The arrow indicates the direction of sound propagation.

3.1. Effective parameter θ_q

Figure 3a shows the ratios $\Theta^* = \theta_{q0}\theta_{p0}^{-1}$ and $\mathcal{Q}^*\Theta^* = \langle Q\rangle_f Q_a^{-1}\theta_{q0}\theta_{p0}^{-1}$ as a function of $b^* = b/s$ for $\varphi = 0$. Small values of b^* mean that the heat source tends to be constant over the whole pore space while larger values indicate that the beam is narrow and therefore the excitation is more localised. The plot shows that when $b^* \to 0$, the static value of the effective parameter θ_q tends to the static thermal permeability. As b^* increases, θ_{q0} becomes larger than θ_{p0}. However, the product between θ_{q0} and the spatially averaged heat source $\langle Q\rangle_f$ decreases as b^* augments, which reflects that narrower beams would lead to a smaller mean local static temperature field $\langle\tau_q\rangle$. Figure 3b shows the behaviour of θ_q/θ_{q0} in frequency. It is clear that θ_q scales with its static value at low frequencies, while at high frequencies, it tends, in a leading order approximation, to $-\mathrm{j}\phi\delta_t^2$. Also, as expected, the behaviour of θ_q in frequency is similar to that of the classical dynamic thermal permeability.

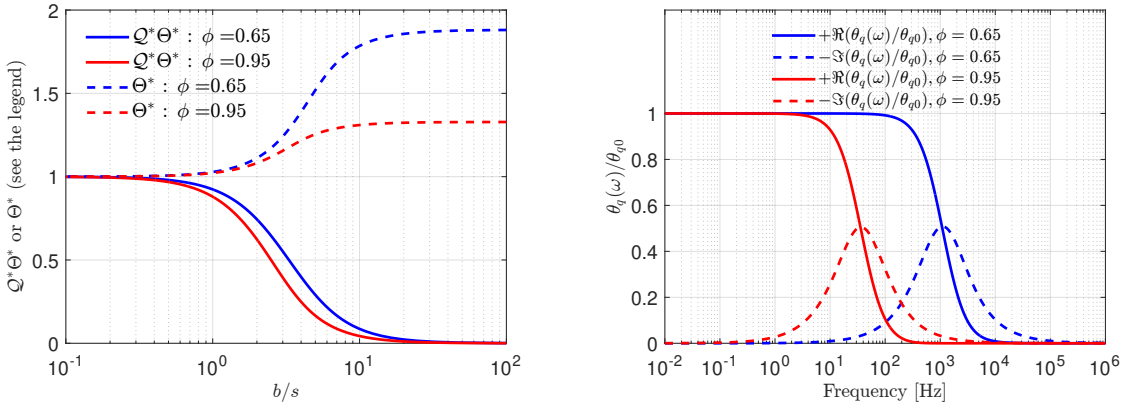

Figure 3: Left – Ratios $\Theta^* = \theta_{q0}/\theta_{p0}$ and $\mathcal{Q}^*\Theta^* = \langle Q\rangle_f\theta_{q0}/\theta_{p0}Q_a$ as a function of $b^* = b/s$. Right – Normalised effective parameter θ_q/θ_{q0} as a function of frequency for $b^* = 4$. The fibre radius is $a = 100\,\mu$m, $\varphi = 0$, and the porosities are $\phi = 0.65$ (blue lines) and $\phi = 0.95$ (red lines).

3.2. Effective sources $H(\omega)$ and $\mathcal{S}(\omega)$

Figure 4 shows the effective sources $H(\omega)$ and $\mathcal{S}(\omega)$ as a function of frequency. The parameters of the material are as in Figure 3. As the frequency increases, the effective source term in the macroscopic mass balance equation, i.e. $H(\omega)$, increases in magnitude until reaching a plateau region for $\omega \gg \omega_{tq}$. When keeping the fibre radius constant, Such a a plateau region starts at a lower frequency in more permeable fibrous media.

The behaviour of the effective source term in the non-homogeneous wave equation, that is $\mathcal{S}(\omega)$, is shown in Figure 4b. Its magnitude increases with frequency while its phase is nearly constant at $-\pi/2$, which is consistent with the asymptotic expressions given by Equations 16 and 17. It is worth mentioning that the effective source $\mathcal{S}(\omega)$ of the material with lower porosity presents higher magnitude. This is because of the larger magnitude of its dynamic density (calculated using the model introduced in [20]) which acts as a filter to the effective source $H(\omega)$.

3.3. Numerical verification

Figure 5 shows the spatially averaged magnitude and phase of the pressure in an air-saturated array of cylinders (with inner heat sources) placed in a $3b \times 3b$ rigid-wall box. In one type of simulations, namely DNS, the pressure was calculated from the solution of the local equations presented in § 2. The other type of simulation, i.e. SUM, consisted in numerically solving the upscaled non-homogeneous wave equation 14, formulated in a $3b \times 3b$ rigid-wall box saturated with a forced effective fluid characterised by its dynamic density $\rho(\omega)$ and compressibility $\mathsf{C}(\omega)$. A good agreement

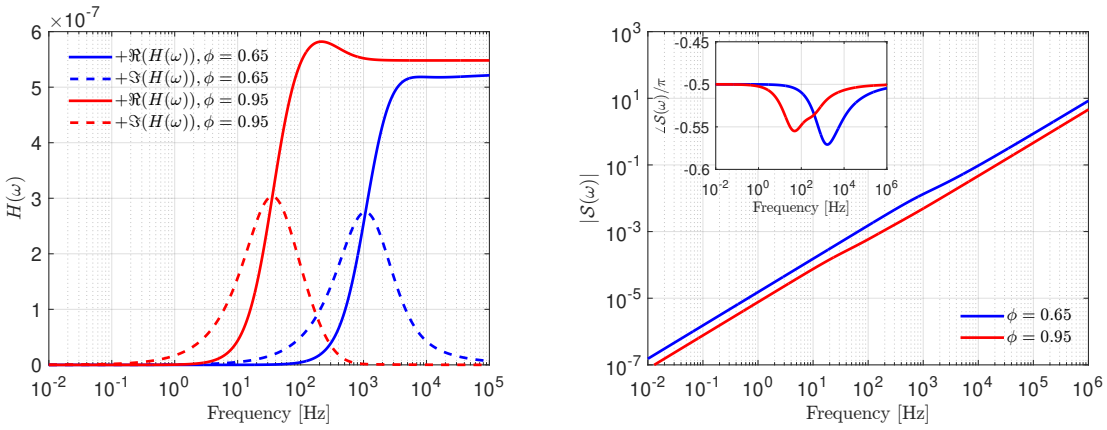

Figure 4: Effective sources $H(\omega)$ (left) and $\mathcal{S}(\omega)$ (right) as a function of frequency. The parameters of the active materials are as in Figure 3.

is found between the results obtained with the two types of simulations, which allows concluding that the developed upscaled theory has been verified. In addition, it is highlighted that the plots show that the sound pressure level L_p is constant at low frequencies and decreases at high frequencies. These trends are well described by Equation 19, which also explains that, when keeping the fibre radius constant, materials with higher porosity emit louder sound at low frequencies due to their larger θ_{q0}, while in denser materials a constant L_p is obtained in a wider frequency range because of their higher ω_q.

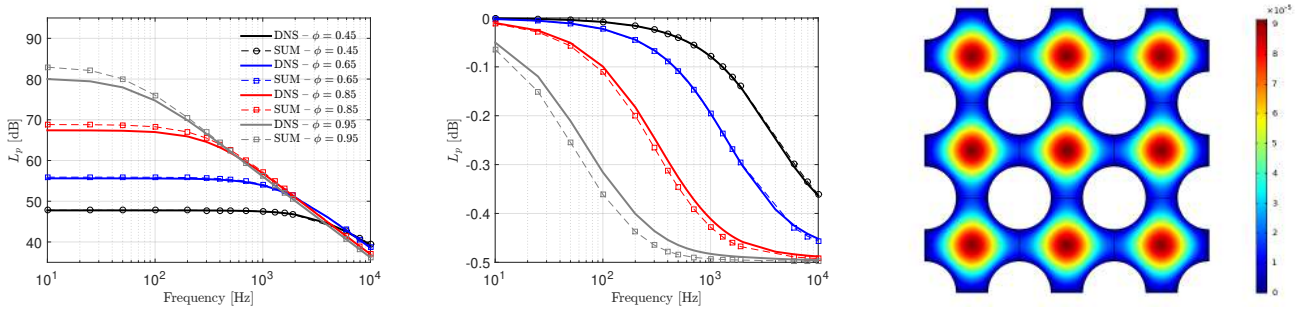

Figure 5: Spatially averaged sound pressure level (left) and phase of pressure (middle) in a $3b \times 3b$ rigid-wall box with an air-saturated array of cylinders with inner heat sources and different porosities. DNS – Direct numerical solution of the local description. SUM – Solution of the upscaled model (i.e. solution of the non-homogeneous Helmholtz equation). The fibre radius is $a = 100$ μm, $Q_a = 1000$ W/m^3 and $b^* = 4$. The local temperature field generated by the inner sources at $f = 100$ Hz in the material with $\phi = 0.65$ is shown on the right-hand side image.

3.4. Acoustic descriptors

Figure 6 shows the reflection and sound absorption coefficients, i.e. R and $\mathcal{A} = 1 - |R|^2$, of 6-cm-thick rigidly-backed layers of an active single porosity material (SPM), an active double porosity composite material (DPM), and their passive counterparts. For the active SPM, the heat sources are placed in the single pore fluid network while for the active DPM the sources are located in the pore fluid network of the porous matrix (subscript m), which is much more permeable than the material the inclusions (subscript i) are made of. In both cases, the inner heat source has parameters $Q_a = 4000$ W/m^3, $b/s = 4$, and φ is varied. As in [15, 16], the matrix is modelled as a fibrous material [20] (with

fibre radius $a_m = 100\ \mu$m and porosity $\phi_m = 0.85$), while the inclusions are made of a highly resistive granular material [21, 22] (with particle radius $a_i = 28\ \mu$m and $\phi_i = 0.32$, leading to a permeability ratio in the order of 10^{-4}). The reflection coefficient was calculated as detailed in [16, 23], with the difference being that the non-homogeneous wave equation 14, instead of the homogeneous Helmholtz equation, was formulated either in the whole effective fluid for the active SPM or in the porous matrix for the active DPM. The amplitude of the incident wave is 0.1 Pa.

The phase of the reflection coefficient for the active and passive materials have similar behaviour. Instead, the magnitude of the reflection for the active SPM with a heat source with $q_a = Q_a e^{j0}$ shows values larger than 1 at low frequencies. This means that the amplitude of the reflected wave has a larger magnitude than that of the incident wave. In consequence, a negative apparent sound absorption coefficient is obtained. A similar trend is observed in the active DPM but $|R| < 1$ occurs at a lower frequency. At higher frequencies, the apparent sound absorption coefficient of the active materials is higher than that of the their passive counterparts. This is primarily attributed to the interaction between the incident and emitted wave which allows obtaining surface impedance values that are closer to those that satisfy the known impedance matching condition. The active materials having $q_a = Q_a e^{j\pi}$, which physically means that the local temperature fields are out of phase, exhibit higher low frequency apparent sound absorption coefficient than their passive counterparts. While it is undeniable that a practical implementation of this phase control concept appears challenging, the presented results do provide evidence of a new mechanism for low frequency sound absorption.

Finally, it is worth highlighting that both R and $\mathcal{A}$ are also highly dependent on the ratio between the amplitude of the incident wave and that of the sound emitted by the porous medium, despite the fact that the introduced upscaled theory is formulated within the framework of linear acoustics.

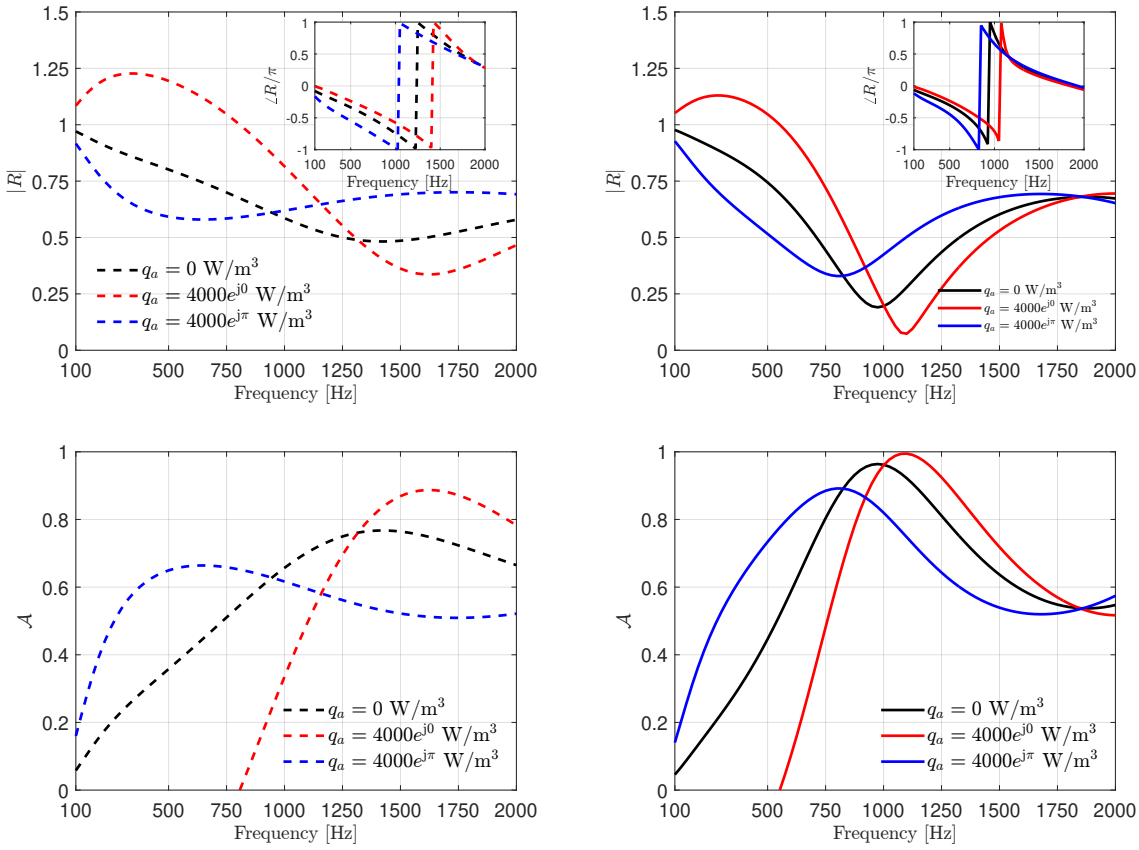

Figure 6: Reflection coefficient (top) and apparent sound absorption coefficient (bottom) of 6-cm rigidly-backed layers of single porosity material (left, dashed lines) and double porosity composite material (right, continuous lines) with active inner volumetric heat sources.

4. CONCLUSIONS

This paper investigated emission and propagation of sound waves in periodic rigid-frame porous media with active inner heat sources. Applying the two-scale asymptotic method of homogenisation to the upscaling of the Stokes-Fourier system with a volumetric heat source as a forcing term in the Fourier's equation, it was found that a macroscopic non-homogeneous wave equation describes the emission and propagation of long sound waves in such active porous media. The analysis of the upscaled model revealed that the general properties of the effective parameters of the effective medium, namely the dynamic density and compressibility, are not altered by the inner heat sources. However, these sources contribute to the effective source term of the upscaled wave equation. Moreover, the developed theory was verified numerically, which allowed evidencing the spectral characteristics of the sound emitted by the porous medium. This work also highlighted the effect of inner heat sources on the acoustic descriptors of single and double porous rigidly-backed active layers, thereby exploring the potential of using the said sources for controlling incident sound waves in a practical configuration.

The results of this work correspond to a first approach to the understanding of the physics of acoustic waves in active multiscale porous media and offer new perspectives for the development of novel active materials for wave engineering in general and noise control in particular.

ACKNOWLEDGEMENTS

This work was supported by the Chilean National Agency for Research and Development (ANID) through FONDECYT Regular Grant 1211310. Support from CeLyA of Université de Lyon operated by ANR (ANR 10 Labex 0060 and ANR 11 IDEX - 0007) is also acknowledged.

REFERENCES

[1] J. L. Auriault, C. Boutin, and C. Geindreau. *Homogenization of Coupled Phenomena in Heterogeneous Media*. ISTE Ltd and John Wiley & Sons, 2009.

[2] G. W. Swift, *Thermoacoustics*, ASA Press, 2017.

[3] H. D. Arnold and I. B. Crandall. The thermophone as a precision source of sound. *Physical Review*, 10: 22–38, 1917.

[4] H. Shinoda, T. Nakajima, K. Ueno, and N. Koshida. Thermally induced ultrasonic emission from porous silicon. *Nature*, 400: 853–855, 1999.

[5] A. O. Niskanen, J. Hassel, M. Tikander, P. Maijala, L. Grönberg, and P. Helistö. Suspended metal wire array as a thermoacoustic sound source. *Applied Physics Letters*, 95: 163102, 2009.

[6] A. E. Aliev, N. K. Mayo, Mo. J. de Andrade, R. O. Robles, S. Fang, R. H. Baughman, M. Zhang, Y. Chen, J. A. Lee, and S. J. Kim. Alternative nanostructures for thermophones. *ACS Nano*, 9 (5): 4743–4756, 2015.

[7] Z. Zhang, H. Tian, P. Lv, Y. Yang, Q. Yang, S. Yang, G. Wang, and T. Ren. High-performance sound source devices based on graphene woven fabrics. *Applied Physics Letters*, 110: 093110, 2017.

[8] Y. Qiao, G. Gou, F. Wu, J. Jian, X. Li, T. Hirtz, Y. Zhao, Y. Zhi, F. Wang, H. Tian, Y. Yang, and T.-L. Ren. Graphene-based thermoacoustic sound. *ACS Nano*, 14: 3779–3804, 2020.

[9] J. L. Auriault, L. Borne, and R. Chambon. Dynamics of porous saturated media, checking of the generalized law of Darcy. *Journal of the Acoustical Society of America*, 77 (5): 1641–1650, 1985.

[10] D. Lafarge, P. Lemarinier, J. F. Allard, and V. Tarnow. Dynamic compressibility of air in porous structures at audible frequencies. *Journal of the Acoustical Society of America*, 102 (4): 1995–2006, 1997.

[11] J. F. Allard and N. Atalla. *Propagation of Sound in Porous Media: Modeling Sound Absorbing Materials*. John Wiley & Sons, 2nd edition, 2009.

[12] L. V. Wang. *Photoacoustic Imaging and Spectroscopy*. CRC Press, 2009.

[13] B. Xia, N. Chen, L. Xie, Y. Qin, and D. Yu. Temperature-controlled tunable acoustic metamaterial with active band gap and negative bulk modulus. *Applied Acoustics*, 112: 1–9, 2016.

[14] C. Olivier , G. Poignand , M. Malléjac , V. Romero-García, G. Penelet, A. Merkel, D. Torrent, J. Li, J. Christensen, and J.-P. Groby. Nonreciprocal and even Willis couplings in periodic thermoacoustic amplifiers. *Physical Review B*, 104: 184109, 2021.

[15] R. Venegas, T. G. Zieliński, G. Núnez, and F.-X. Bécot. Acoustics of porous composites. *Composites part B Engineering*, 220: 109006, 2021.

[16] G. Núnez, R. Venegas, T. G. Zieliński, and F.-X. Bécot. Equivalent fluid approach to modeling the acoustical properties of polydisperse heterogeneous porous composites. *Physics of Fluids*, 33: 062008, 2021.

[17] X. Olny and C. Boutin. Acoustic wave propagation in double porosity media. *Journal of the Acoustical Society of America*, 113 (6): 73–89, 2003.

[18] R. Venegas and O. Umnova. Acoustical properties of double porosity granular materials. *Journal of the Acoustical Society of America*, 130 (5): 2765–2776, 2011.

[19] P. M. Morse and K. U. Ingard, *Theoretical Acoustics*, Princeton University Press, 1986.

[20] O. Umnova, D. Tsiklauri, and R. Venegas. Effect of boundary slip on the acoustical properties of microfibrous materials. *Journal of the Acoustical Society of America*, 126: 1850–1861, 2009.

[21] C. Boutin and C. Geindreau. Estimates and bounds of dynamic permeability of granular media. *Journal of the Acoustical Society of America*, 124: 3576–3593, 2008.

[22] C. Boutin and C. Geindreau. Periodic homogenization and consistent estimates of transport parameters through sphere and polyhedron packings in the whole porosity range. *Physical Review E*, 82: 036313, 2010.

[23] T. G. Zielinski, R. Venegas, C. Perrot, M. Cervenka, F. Chevillotte, and K. Attenborough. Benchmarks for microstructure-based modelling of sound absorbing rigid-frame porous media. *Journal of Sound and Vibration*, 483: 115441, 2020.